Temperature-sensitive ductilization in hydrogen-alloyed Fe-Cr-Ni austenitic steel by enhanced deformation twinning

Yuhei Ogawa[a]

a Research Center for Structural Materials, National Institute for Materials Science (NIMS), 1-2-1 Sengen, Tsukuba, 305-0047, Japan

E-mail: OGAWA.yuhei@nims.go.jp

Abstract

Solute hydrogen (H) is recently identified to improve the strength and ductility of some Fe-Cr-Ni austenitic steels due to a combination of solid-solution hardening and accelerated deformation twinning. In the present study, the impact of deformation temperature (173~373 K) on this ductilization effect was studied primarily under a slow strain rate in Fe-24Cr-19Ni steel pre-charged with 7570 at ppm H. Ambient temperature was found to be an optimized condition where H-induced ductilization was the most pronounced. With the lowering temperature below 200 K, ductilization was mitigated entirely in spite of still substantial H-induced twinning enhancement. The result was ascribed to an overly prompted twinning activity and its premature density saturation, encompassing a consummation of work-hardenability at an earlier deformation stage.

Keywords: Austenitic steels; Hydrogen; Twinning; Temperature; Ductility

The ductility improvement in hydrogen (H)-alloyed Fe-Cr-Ni austenitic steels [1,2] is a phenomenon potentially breaking through the tenet on H as a destructive element for the mechanical properties of metals [3,4]. The outcome stems from H-enhanced deformation twinning, retaining work-hardenability, and retarding the onset of plastic instability [5–7]. Although there are compositional requirements to control austenite phase stability and stacking fault energy (SFE) for its manifestation, ductilization is desirable to develop H-compatible materials applied to a forthcoming carbon-neutral society. The strategy utilizing such a specific deformation mode is reminiscent of twinning-induced plasticity (TWIP) steels, the example of which is Fe-Mn-based alloys [8]. In line with it, here we define the terminology “H-TWIP” to signify the accelerated

twinning-induced plasticity under the presence of H.

Besides the importance of chemical composition, the deformation twinning in face-centered cubic (FCC) metals is microstructurally and environmentally sensitive [9–12]. Crucial factors in conventional polycrystals are grain size and texture, wherein coarser grain reduces critical stress/strain for twin nucleation [12], as well as twinning prevails in <111>-oriented grains [11]. Moreover, increasing temperature retards twinning and diminishes saturated twin density owing to SFE escalation [9], a parameter determining the separation distance between partial dislocations [13] which act as twin embryos [14]. Integrated optimization of material parameters concerning the targeted temperature range is a vital attempt to effectively use TWIP as a ductility improver. Nevertheless, research on the twinning in H-alloyed austenitic steels [1,5,15–17] is in its infancy, leaving plural assignments in identifying the requirements for concomitant ductilization.

Apart from the H-impact, Koyama et al. established systematic insights into the temperature effect on twinning and ductility in Fe-18Mn-1.2C steel [18]. They unveiled ductility maximization under an intermediate temperature range, where twinning commenced at a later deformation stage and continuously increased their density until the plastic instability point. When the temperature was lower, ductility decreased in spite of substantial twinning. This was due to an earlier onset of twining and its premature saturation, interrupting work-hardenability retention at a minor strain [18]. Given this, the ductility improvement in H-alloyed austenitic steels [1,15–17] should also not be invariant but rather temperature-dependent. Also, it is a tentative belief that H-TWIP primarily relies on the dynamic interactions between diffusible H and dislocations [1,5,15,17], a phenomenon similarly susceptible to temperature.

In our previous paper, we selected Type310S (Fe-24Cr-19Ni) steel doped with 7570 at ppm H; the temperature-dependent yield stress was evaluated under 173 to 423 K [19]. This paper targets the same material and testing conditions while the focus shifts to larger strain where twinning contributes substantially to plasticity. H-induced changes in uniform and fracture elongation were elaborated in terms of twin density, twinning stress/strain, and work-hardening at each temperature. The strain rate effect was subsidiarily studied at 173 K to screen the essence of dynamic H-dislocation interactions.

A Type310S steel, in which H-TWIP and ductilization manifested [1,2,5], was used. For the details of the material and specimen, the readers shall refer to [19]. Tensile tests

were conducted at 173~373 K with an initial strain rate of 5×10^{-5}/s and/or 5×10^{-3}/s. A screw-driven electromechanical test frame was employed with a strain measurement by a linear variable differential transformer (LVDT). The ϕ6-mm tensile specimens were uniformly H-charged *via* thermal exposure to pressurized H_2 gas at 100 MPa and 543 K. Thermal desorption analysis revealed that the H concentration was 7570 at ppm [19].

The deformation microstructures in uniformly deformed parts of fractured specimens were analyzed by electron backscattered diffraction (EBSD). The mid-diameter and ±1 mm apart from there were selected for the field of view. A JEOL JSM-7001F scanning electron microscope (SEM) was used for EBSD at an acceleration voltage of 15 kV and a beam step size of 150 nm. The total length of Σ3 coincident site lattice (CSL) boundaries was measured to determine deformation twin density.

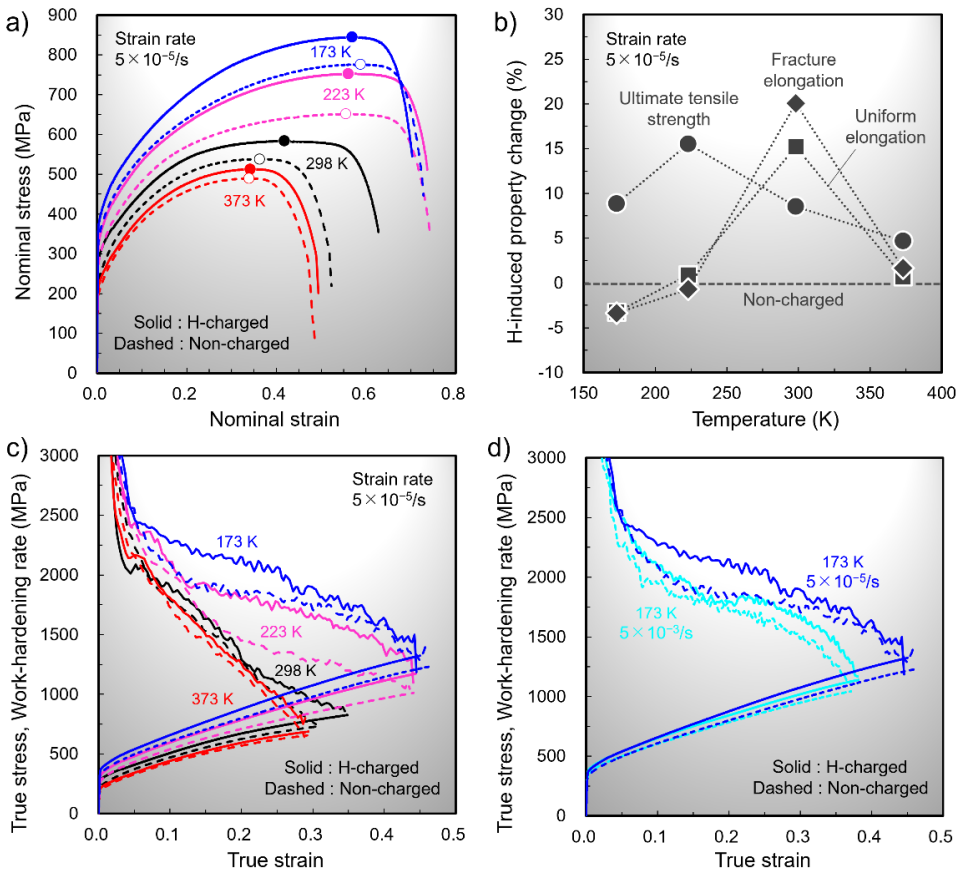

Fig. 1 (a) Nominal and (c)(d) true stress-strain curves of non-charged and H-charged specimens at 173~373 K under strain rate of 5×10^{-5} and/or 5×10^{-3}/s. The work-hardening rate (WHR) curves are included in (c) and (d). The dots on the stress-strain curves in (a) denote the end of uniform elongation. (b) summarizes strength and ductility parameters of H-charged specimens, which were normalized by those in non-charged specimens.

The nominal stress-strain curves of non-charged and H-charged specimens under a strain rate of 5×10^{-5}/s are shown in Fig. 1 (a). Irrespective of the presence and absence of H, overall stress-strain curves exhibited an upward shift with the decrease in temperature owing to the thermally activated character of dislocation mobility [20], and the fracture elongation was maximized at 223 K. The H-induced increases of flow stress, as well as enhanced uniform and fracture elongations [1,2], were reproduced at 298 K, while higher temperatures (373 K) tended to mitigate all these H-effects. At lower temperatures of 223 and 173 K, the flow stress augmentation by H was still substantial. However, H-assisted ductilization totally disappeared, and the elongation of the H-charged specimen became slightly inferior to the non-charged one at 173 K. The percentages of H-induced changes in ultimate tensile strength, uniform elongation, and fracture elongation are summarized in Fig. 1 (b).

The data in Fig. 1 (a) were converted into true stress-strain curves, and work-hardening rate (WHR) curves in Fig. 1 (c). The impact of H on the WHR was marginal at 298 K at the beginning to intermediate stages of deformation, then an upward deviation of WHR by H was recognized under strain over 0.2. Such an escalation of WHR stems from H-TWIP, responsible for the improved elongation at this temperature [1,2,5]. Comparing non-charged specimens to each other, lowering the temperature caused similar deviations of WHR curves, even at smaller strains of 0.1~0.2, from the one at 298 K; an outcome ascribed to the temperature-dependent decrease of SFE in Fe-Cr-Ni system [21]. Notably, the H-effect in escalating WHR was still significant at 173 and 223 K, wherein the deviating point of WHR from the non-charged specimen shifted toward a smaller strain as the temperature decreased. This result implies that H-TWIP was similarly operational at temperatures lower than 298 K. However, once after the escalation occurred, the gap of WHR between non-charged and H-charged specimens decayed as the deformation progressed, finally merging at or slightly before the plastic instability. The effect of increasing strain rate on the stress-strain behavior at 173 K is subsidiarily presented in Fig. 1 (d). Albeit the presence of H was more or less capable of escalating WHR at a strain around 0.1 even under a faster strain rate of 5×10^{-3}/s, its extent was small as compared with 5×10^{-5}/s case, an indication of the weakening of H-TWIP. Note that the lowering of WHR by faster straining in both non-charged and H-charged

specimens at the strain range larger than 0.2 might be due to deformation heat, an influence of which became more significant in such later deformation stage where heat dissipation gradually became incapable to compansate the heating.

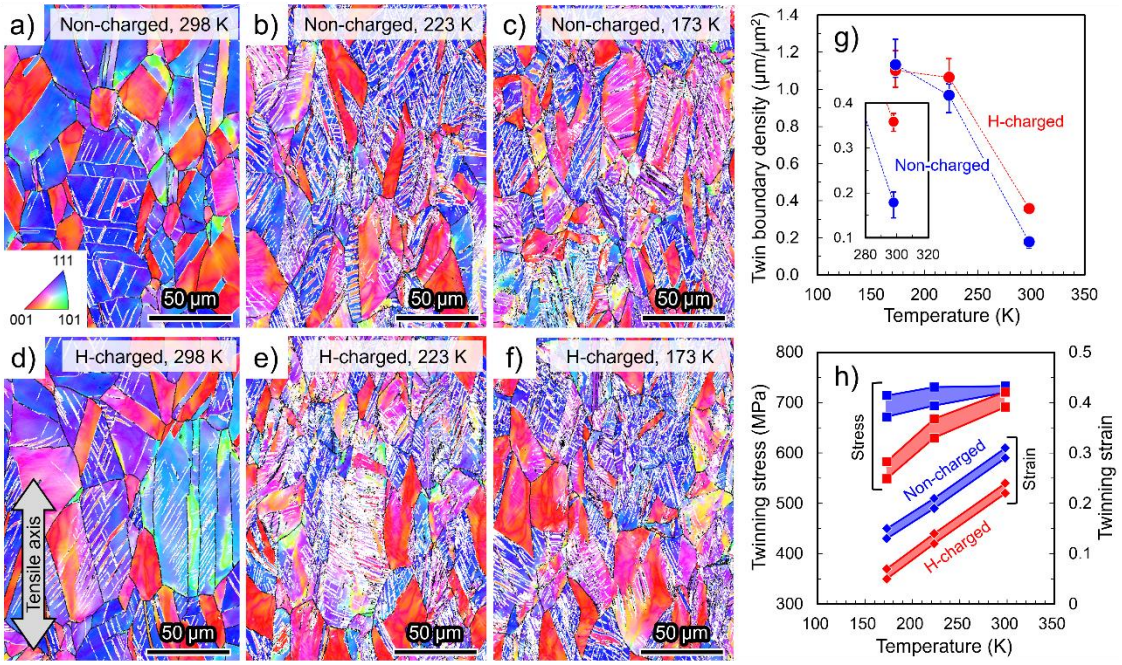

Fig. 2 (a)~(f) EBSD inverse pole figure maps with respect to the tensile axis in the uniformly deformed parts of (a)~(c) non-charged and (d)~(f) H-charged specimens fractured at (a)(d) 298 K, (b)(e) 223 K, and (c)(f) 173 K. The white lines delineate Σ3 twin boundaries. The areal density of twin boundaries measured by EBSD, as well as critical stress and strain for the twinning evolution are depicted in (g) and (h).

Fig. 2 (a)~(f) showcase the EBSD inverse pole figure maps of the deformation microstructures in non-charged and H-charged specimens at 173~298 K. Deformation as well as annealing twins are visible as the Σ3 CSL boundaries delineated by white lines, the density of which evidently increased with the decrease of temperature. The amount of deformation twins was negligible at 373 K as anticipated from the stress-strain properties in Fig. 1. Besides, FCC phase was stable, and no phase transformation occurred even at 173 K, as confirmed by X-ray diffraction analysis on the fractured specimens. In Fig. 2 (g), the twin densities at the plastic instability points are plotted as a function of test temperature. Each plot point was constructed from three EBSD micrographs for statistical significance. The twin density was amplified two-fold by H at 298 K. On the other hand, the densities in non-charged and H-charged specimens were mutually identical within the error bands at 173 and 223 K, although their absolute values far exceeded those at 298 K.

The critical twinning stress and strain are key perspectives when attempting to elaborate TWIP-mediated property changes [9,14]. Extraction of those criteria from stress-strain curves is quite challenging, requiring a distinguishment on where twinning started to overlap the WHR contribution from dislocations. Additionally, WHR depends not only on H but also temperature itself [22,23]. The latter makes the deviation point on WHR curves, which is correlated with twin activity, not straightforward.

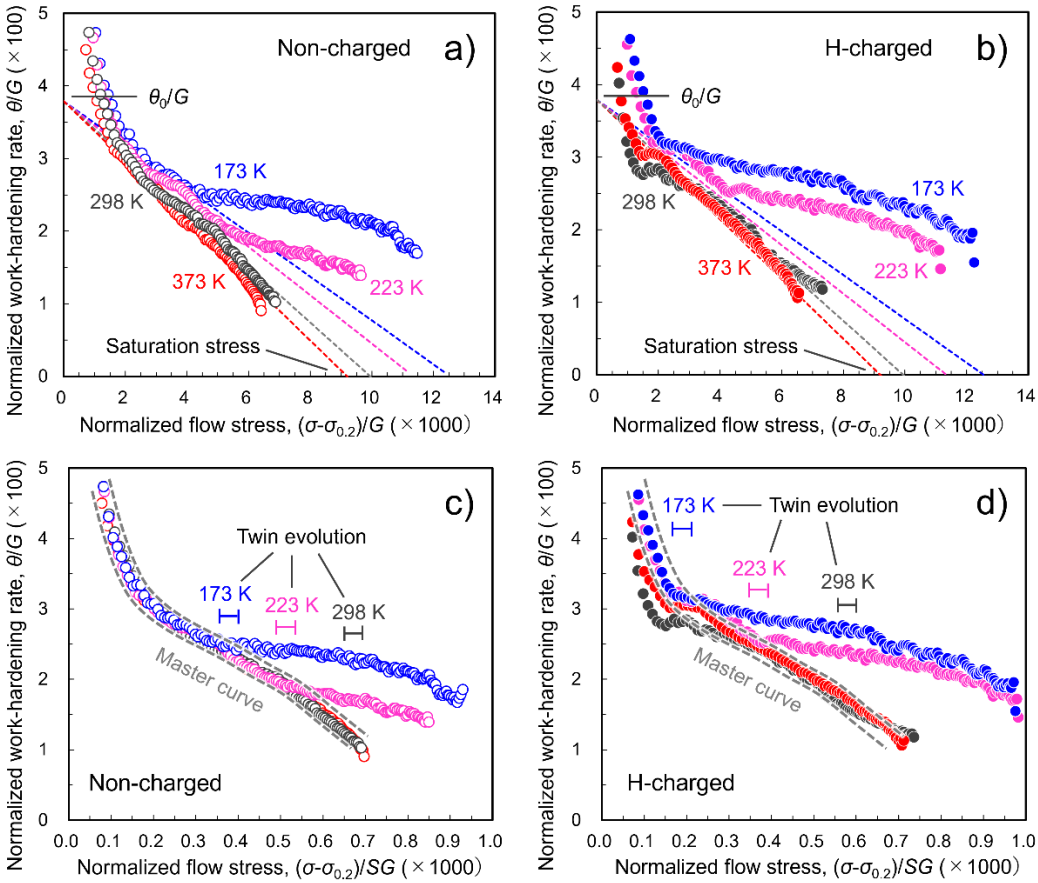

Fig. 3 (a)(b) Relationship between work-hardening rate and flow stress both normalized by shear modulus for (a) non-charged and (b) H-charged specimens. The curves in (a) and (b) are reproduced in (c) and (d) with the abscissa scaled by saturation stress according to the method established by Kocks and Mecking [24]. The deviation from the master curves potentially corresponds to the progressing evolution of deformation twins.

Here, we used the procedure established by Kocks and Mecking [24] for assembling the WHRs at different temperatures into a unified master curve. WHR, θ, in FCC metals under applied stress, σ, generally obeys the following Voce law [24].

$$\theta = \theta_0\left(1 - \frac{\sigma}{\sigma_v}\right) \quad (1)$$

Here, θ_0 is the Stage II hardening rate (*i.e.*, ~G/200, where G is shear modulus), and σ_v is saturation stress at which accumulation and annihilation of dislocations are balanced. In line with eq. (1), WHRs are plotted versus flow stress, σ, in Fig. 3 (a) and (b). For compensating the influences of temperature-dependent G [23] and strengthening factors other than dislocations (*e.g.*, grain boundaries and solute atoms), both axes were normalized by G, and 0.2% proof stress, $\sigma_{0.2}$, was subtracted from σ on the abscissa. Longtail linearity between θ/G and $(\sigma-\sigma_{0.2})/G$ was seen at 298 and 373 K, aside from the high WHR at small $(\sigma-\sigma_{0.2})/G$. At 173 and 223 K, this linear portion became shorter. The back extrapolation of those linear parts yields θ_0/G as an ordinate intercept, which should be temperature-independent owing to an athermal character of θ_0 [23]. Meanwhile, their extrapolation toward $\theta/G = 0$ on abscissa assigns $S = (\sigma_v-\sigma_{0.2})/G$, a scaling parameter used for the unification.

In Fig. 3 (c) and (d), Fig. 3 (a) and (b) are reproduced with the normalization of abscissa by S. Some WHR curves in H-charged specimens possessed complex shapes due to temporal WHR drop after yielding, which is potentially due to dragging of H atmosphere on mobile dislocations [19]. The linear fitting was thereby unsuccessful. Thus, the S parameters at each temperature were taken to be identical to those in non-charged samples, an assumption validated by the fact that internal deformation structure is not largely affected by H before twinning [1,5,25]. In non-charged specimens (Fig. 3 (c)), the conformity between WHR curves at different temperatures was elegant *via* scaling with S, visualizing the deviation from this unified master curve at 173 and 223 K now explicitly (*i.e.*, $(\sigma_v-\sigma_{0.2})/SG$ = 0.50~0.55 and 0.30~0.35 for 223 and 173 K, respectively). The appropriateness of the selection of S is discussed in Supplementary Material S1.

Since eq. (1) only considers plasticity carried by dislocations, the deviation from the master curve potentially reflects that the contribution of deformation twinning to WHR became significant. Fig. 2 (h) shows the twinning stress estimated through this procedure. Note that the deviation was unclear in the non-charged specimen at 298 K, even though twins were moderately observed in Fig. 2 (a). For the sake of expedience, the stress and strain around the end of uniform deformation, at which Fig. 2 (a) was captured, was taken as the critical values for twinning. Such an absence of curve deviation is due to the smaller amounts of twins and their insufficient impact on WHR. This makes a caution that the twinning stress and strain in Fig. 2 (h) corresponds not exactly to the initiation of twins

but rather an achievement of certain twin density and configuration (*i.e.*, they should be called twin evolution stress and strain). Indeed, an *in-situ* observation revealed that the deviation in WHR emerged when twins decently evolved and started intersecting with each other [5]. The same master curve was installed to the H-charged case, and twinning stress was extracted likewise (Fig. 2 (h)). Albeit our method provides merely rough approximations, functions of H to reduce twin evolution stress and strain were apparent, the former of which amplified with decreasing temperature. The greater H impact on the twin evolution stress at lower temperatures might be superficial according to steeper slopes of stress-strain curves at smaller strain. An almost constant gap of the twin evolution strain between non-charged and H-charged specimens infers that strain is a more important criterion than stress for interpreting the rationale of H-TWIP.

Fig. 1 unveiled that the H-induced ductilization phenomenon is substantially temperature-dependent. Although enhanced WHR, potentially due to H-TWIP, manifested at temperatures below 298 K, it increased neither uniform nor fracture elongations (Fig. 1 (b) and (c)). The absence of ductilization despite an accelerated twinning is interpreted equivalently to the discussion framework in [18]. That is, rapid twin evolution due to decreasing critical strain (Fig. 2 (h)) encompassed an earlier saturation of twin density, prematurely consuming TWIP-aided work-hardenability. Indeed, the twin densities in non-charged and H-charged specimens at 223 and 173 K were mutually identical at the end of uniform deformation. An important implication of Fig. 2 (g) is that the maximum twin density in the present material lies around 1.0~1.2 $\mu m/\mu m^2$ and is not largely affected by H. Ultimately, the requirement for the advent of H-induced ductilization is now defined: the material-specific maximum twin density, a consummation of which is hastened by H-TWIP, should not be reached until the plastic instability commences. At 298 K where the focus has been placed in our preceding studies [1,2], such an optimized condition had incidentally been satisfied.

The twin evolution in FCC metals comprises a nucleation process through specific interactions between extended dislocations and their subsequent propagation [9,26–28]. It is the former event for H-TWIP wherein diffusible H is presumed to play vital roles *via* coordinatively migrating with mobile dislocations [1,15,17]. Accelerated nucleation augments the twin density under a given strain, prompting the deviation from the Voce master curve. Even though microscale sequences of twin nucleation and growth are

beyond the scope of this paper, an almost fixed decrease in the twin evolution strain by H (Fig. 2 (h)) fortunately provides us one prospect to recall an assertion made in our previous work [5]. Namely, the primary function of H is to increase the probability for twin embryos to grow into nuclei, when the sufficient density of dislocations, which may depend on SFE (*i.e.*, temperature), is reached. Furthermore, what was noteworthy is that the enhancement in twin evolution also happened at 173 K, where the dynamic interaction of H with moving dislocations should not be operational [19]. Only weak segregation is anticipated under a strain rate of 5×10^{-5}/s (see Supplementary Material S2 [29–31]), compelling us to account for such imperfect interaction as a factor enough to be an H-TWIP trigger. This last statement is supported by the diminished H-impact on WHR at a strain rate of 5×10^{-3}/s (Fig. 1 (d)), at which interaction between H and dislocations is almost infeasible. In conventional TWIP steel, an enhanced twinning by interstitials was attributed to the pinning of trailing partial dislocations, whereas leading partials can move freely [32]. An elucidation has been performed for Fe-Mn-C steel, invoking the applicability of a similar description to H-alloyed Fe-Cr-Ni alloy since the model does not require any complete equilibration of H around mobile dislocations. To deepen our understanding, real-time characterization of dislocations, stacking fault densities, and twin evolution is desired, for example, by cryogenic tensile tests equipped with neutron diffraction [33,34]. Also note that deformation twinning triggers hydrogen embrittlement accompanying intergranular or twin boundary fracture especially in TWIP steels containing large amount of Mn [35]. This is because high Mn content may lower interatomic bond, promoting inferface decohesion under the presence of H [36]. Under a given H concentration, the present material possibly exhibited superior resistance to such embrittlement due to its low Mn content around 1 mass % [19]. If the H concentration became further greater, an embrittlement similar to high-Mn steels would manifest even in Type310S steel, as indeed observed under severe cathodic H-charging [37].

The temperature-dependence of the ductilization by solute H was studied under 173~373 K and slow strain rate in Fe-24Cr-19Ni steel uniformly charged with 7570 at ppm H. Amongst the examined temperatures, 298 K was found to be an optimized condition where H-induced ductilization *via* an enhanced deformation twinning (H-TWIP) was maximally pronounced. By lowering the temperature below 200 K, the ductilization was mitigated. The result was ascribed to an overly prompted twin activity

and its premature saturation, encompassing a consummation of work-hardenability at an earlier deformation stage. A faster strain rate at 173 K suppressed the manifestation of H-TWIP. These overall temperature and strain rate effects offered a direction for further study to elaborate the underlying rationales of H-TWIP, a fruitful phenomenon in attempting to develop epoch-making structural steels for H-bearing applications.

Acknowledgements

This work was supported by JSPS KAKENHI (Grant Number: 21K14045), as well as financial support from JFE 21st Century Foundation and The Iwatani Naoji Foundation. The author is grateful to the members of the Kobe Materials Testing Laboratory (KMTL) group in Japan for their kind experimental support. Dr. Kaneaki Tsuzaki from National institute for Materials Science and Prof. Osamu Takakuwa from Kyushu University are also greatly acknowledged for their helpful discussion related to this research.

References

[1] Y. Ogawa, H. Hosoi, K. Tsuzaki, T. Redarce, O. Takakuwa, H. Matsunaga, Hydrogen, as an alloying element, enables a greater strength-ductility balance in an Fe-Cr-Ni-based, stable austenitic stainless steel, Acta Mater. 199 (2020) 181–192. https://doi.org/10.1016/j.actamat.2020.08.024.

[2] H. Nishida, Y. Ogawa, K. Tsuzaki, Chemical composition dependence of the strength and ductility enhancement by solute hydrogen in Fe–Cr–Ni-based austenitic alloys, Materials Science and Engineering: A. 836 (2022) 142681. https://doi.org/10.1016/j.msea.2022.142681.

[3] M.B. Djukic, G.M. Bakic, V.S. Zeravcic, A. Sedmak, B. Rajicic, Hydrogen embrittlement of industrial components: Prediction, prevention, and models, Corrosion. 72 (2016) 943–961. https://doi.org/10.5006/1958.

[4] J.P. Hirth, Effects of hydrogen on the properties of iron and steel, Metallurgical Transactions A. 11 (1980) 861–890. https://doi.org/10.1007/BF02654700.

[5] Y. Ogawa, H. Nishida, O. Takakuwa, K. Tsuzaki, Hydrogen-enhanced deformation twinning in Fe-Cr-Ni-based austenitic steel characterized by in-situ EBSD observation, Mater Today Commun. 34 (2023) 105433. https://doi.org/10.1016/j.mtcomm.2023.105433.

[6] O. Bouaziz, S. Allain, C. Scott, Effect of grain and twin boundaries on the hardening mechanisms of twinning-induced plasticity steels, Scr Mater. 58 (2008) 484–487. https://doi.org/10.1016/j.scriptamat.2007.10.050.

[7] L. Rémy, The interaction between slip and twinning systems and the influence of twinning on the mechanical behavior of fcc metals and alloys, Metallurgical Transactions A. 12 (1981) 387–408. https://doi.org/10.1007/BF02648536.

[8] B.C. De Cooman, Y. Estrin, S.K. Kim, Twinning-induced plasticity (TWIP) steels, Acta Mater. 142 (2018) 283–362. https://doi.org/10.1016/j.actamat.2017.06.046.

[9] L. Remy, Kinetics of f.c.c. deformation twinning and its relationship to stress-strain behaviour, Acta Metallurgica. 26 (1978) 443–451. https://doi.org/10.1016/0001-6160(78)90170-0.

[10] I. Karaman, H. Sehitoglu, K. Gall, Y.I. Chumlyakov, H.J. Maier, Deformation of single crystal Hadfield steel by twinning and slip, Acta Mater. 48 (2000) 1345–1359.

https://doi.org/10.1016/S1359-6454(99)00383-3.
[11] I. Gutierrez-Urrutia, S. Zaefferer, D. Raabe, The effect of grain size and grain orientation on deformation twinning in a Fe–22wt.% Mn–0.6wt.% C TWIP steel, Materials Science and Engineering: A. 527 (2010) 3552–3560. https://doi.org/10.1016/j.msea.2010.02.041.
[12] E. El-Danaf, S.R. Kalidindi, R.D. Doherty, Influence of grain size and stacking-fault energy on deformation twinning in fcc metals, Metallurgical and Materials Transactions A. 30 (1999) 1223–1233. https://doi.org/10.1007/s11661-999-0272-9.
[13] C.G. Rhodes, A.W. Thompson, The composition dependence of stacking fault energy in austenitic stainless steels, Metallurgical Transactions A. 8 (1977) 1901–1906. https://doi.org/10.1007/BF02646563.
[14] T.S. Byun, On the stress dependence of partial dislocation separation and deformation microstructure in austenitic stainless steels, Acta Mater. 51 (2003) 3063–3071. https://doi.org/10.1016/S1359-6454(03)00117-4.
[15] C. Zhang, H. Zhi, S. Antonov, L. Chen, Y. Su, Hydrogen-enhanced densified twinning (HEDT) in a twinning-induced plasticity (TWIP) steel, Scr Mater. 190 (2021) 108–112. https://doi.org/10.1016/j.scriptamat.2020.08.047.
[16] H. Luo, Z. Li, D. Raabe, Hydrogen enhances strength and ductility of an equiatomic high-entropy alloy, Sci Rep. 7 (2017) 9892. https://doi.org/10.1038/s41598-017-10774-4.
[17] K. Yamada, M. Koyama, T. Kaneko, K. Tsuzaki, Positive and negative effects of hydrogen on tensile behavior in polycrystalline Fe–30Mn–(6 −x)Si–xAl austenitic alloys, Scr Mater. 105 (2015) 54–57. https://doi.org/10.1016/j.scriptamat.2015.05.007.
[18] M. Koyama, T. Sawaguchi, K. Tsuzaki, TWIP Effect and Plastic Instability Condition in an Fe-Mn-C Austenitic Steel, ISIJ International. 53 (2013) 323–329. https://doi.org/10.2355/isijinternational.53.323.
[19] Y. Ogawa, O. Takakuwa, K. Tsuzaki, Solid-solution hardening by hydrogen in Fe–Cr–Ni-based austenitic steel: Temperature and strain rate effects, Materials Science and Engineering: A. (2023) 145281. https://doi.org/10.1016/j.msea.2023.145281.
[20] D. Hull, D.J. Bacon, Introduction to Dislocations, 3rd ed., Butterworth-Heinemann, 2011. https://doi.org/10.1016/C2009-0-64358-0.
[21] R.M. Latanision, A.W. Ruff, The temperature dependence of stacking fault energy in Fe-Cr-Ni alloys, Metallurgical Transactions. 2 (1971) 505–509. https://doi.org/10.1007/BF02663341.
[22] P.S. Follansbee, U.F. Kocks, A constitutive description of the deformation of copper based on the use of the mechanical threshold stress as an internal state variable, Acta Metallurgica. 36 (1988) 81–93. https://doi.org/10.1016/0001-6160(88)90030-2.
[23] H. Mecking, U.F. Kocks, Kinetics of flow and strain-hardening, Acta Metallurgica. 29 (1981) 1865–1875. https://doi.org/10.1016/0001-6160(81)90112-7.
[24] U.F. Kocks, H. Mecking, Physics and phenomenology of strain hardening: the FCC case, Prog Mater Sci. 48 (2003) 171–273. https://doi.org/10.1016/S0079-6425(02)00003-8.
[25] K. Kamei, Y. Koumura, A. Macadre, K. Goda, Quantitative Evaluation of Solute Hydrogen Effect on Dislocation Density in a Low-carbon Stable Austenitic Stainless Steel, ISIJ International. 61 (2021) 1736–1738. https://doi.org/10.2355/isijinternational.ISIJINT-2020-677.
[26] S. Mahajan, G.Y. Chin, Formation of deformation twins in f.c.c. crystals, Acta Metallurgica. 21 (1973) 1353–1363. https://doi.org/10.1016/0001-6160(73)90085-0.
[27] J.B. Cohen, J. Weertman, A dislocation model for twinning in f.c.c. metals, Acta Metallurgica. 11 (1963) 996–998. https://doi.org/10.1016/0001-6160(63)90074-9.
[28] H. Fujita, T. Mori, A formation mechanism of mechanical twins in F.C.C. Metals, Scripta Metallurgica. 9 (1975) 631–636. https://doi.org/10.1016/0036-9748(75)90476-7.
[29] S. Harper, Precipitation of Carbon and Nitrogen in Cold-Worked Alpha-Iron, Physical Review. 83 (1951) 709–712. https://doi.org/10.1103/PhysRev.83.709.
[30] T. Perng, C.J. Altstetter, Effects of deformation on hydrogen permeation in austenitic stainless steels, Acta Metallurgica. 34 (1986) 1771–1781. https://doi.org/10.1016/0001-6160(86)90123-9.
[31] A. Atrens, N.F. Fiore, K. Miura, Dislocation damping and hydrogen pinning in austenitic

stainless steels, J Appl Phys. 48 (1977) 4247–4251. https://doi.org/10.1063/1.323410.
[32] M. Koyama, T. Sawaguchi, K. Tsuzaki, Influence of Dislocation Separation on Dynamic Strain Aging in a Fe-Mn-C Austenitic Steel, Mater Trans. 53 (2012) 546–552. https://doi.org/10.2320/matertrans.M2011342.
[33] J.S. Jeong, W. Woo, K.H. Oh, S.K. Kwon, Y.M. Koo, In situ neutron diffraction study of the microstructure and tensile deformation behavior in Al-added high manganese austenitic steels, Acta Mater. 60 (2012) 2290–2299. https://doi.org/10.1016/j.actamat.2011.12.043.
[34] W. Woo, M. Naeem, J.-S. Jeong, C.-M. Lee, S. Harjo, T. Kawasaki, H. He, X.-L. Wang, Comparison of dislocation density, twin fault probability, and stacking fault energy between CrCoNi and CrCoNiFe medium entropy alloys deformed at 293 and 140K, Materials Science and Engineering: A. 781 (2020) 139224. https://doi.org/10.1016/j.msea.2020.139224.
[35] M. Koyama, E. Akiyama, Y.K. Lee, D. Raabe, K. Tsuzaki, Overview of hydrogen embrittlement in high-Mn steels, Int J Hydrogen Energy. (2017). https://doi.org/10.1016/j.ijhydene.2017.02.214.
[36] M. Koyama, H. Wang, V.K. Verma, K. Tsuzaki, E. Akiyama, Effects of Mn Content and Grain Size on Hydrogen Embrittlement Susceptibility of Face-Centered Cubic High-Entropy Alloys, Metallurgical and Materials Transactions A. 51 (2020) 5612–5616. https://doi.org/10.1007/s11661-020-05966-z.
[37] H. Ji, I.-J. Park, S.-M. Lee, Y.-K. Lee, The effect of pre-strain on hydrogen embrittlement in 310S stainless steel, J Alloys Compd. 598 (2014) 205–212. https://doi.org/10.1016/j.jallcom.2014.02.038.